

# Wavelet Analysis of Electrochemical Noise Measurements During Atmospheric Corrosion of Mild Steel in the Simulated Marine Environment

Lihua Dang<sup>1</sup>, Zhiming Gao<sup>2,\*</sup>, Xinyue Wang<sup>2</sup>, Chen Wei<sup>1</sup>, Lianheng Han<sup>2</sup>, Jianguo Chen<sup>1</sup>

<sup>1</sup>Tianjin Special Equipment Inspection Institute, Tianjin, 300192, China;

<sup>2</sup>School of Material Science and Technology, Tianjin University, Tianjin, 300072, China

\*E-mail: [gaozhiming@tju.edu.cn](mailto:gaozhiming@tju.edu.cn)

Received: 7 January 2020/ Accepted: 26 February 2020 / Published: 10 April 2020

---

In this paper, the wavelet decomposition of the electrochemical noise was successfully applied to derive the wavelet noise resistance ( $R_{cd}$ ), which was further used to assess the corrosion behavior of Q235 mild steel in the simulated corrosion atmosphere (the salt spray test with 0.01 and 0.1 mol/L NaCl). The noise signatures, noise resistance ( $R_n$ ), SEM, and XRD techniques were used as complementary measurements. The electrochemical noise data were acquired from two identical working electrodes by the zero resistance ammeter (ZRA) mode. The experimental results of the noise signatures and  $R_n$  indicated that the corrosion rate increased with the exposure time in the early stages of atmospheric corrosion. The analysis of the surface corrosion morphology and  $R_n$  showed a higher corrosion rate at a higher concentration of spraying solution. Also, the values of  $R_n$  and  $R_{cd}$  closing to the 2 Hz corroborate well in both simulated corrosion atmospheres. The wavelet noise resistance is an effective method for the analysis of the atmospheric corrosion damage of Q235 steel in the marine environment.

---

**Keywords:** Mild steel, electrochemical noise, atmospheric corrosion.

## 1. INTRODUCTION

Atmospheric corrosion, as a most prevalent corrosion type, readily deteriorates different kinds of exposed objects, such as engineering structures and devices [1-7]. Mild steel (Q235) is a widely used construction material of choice for engineering products like rib reinforcements, bridges, boilers, and containers. However, the global problem is that mild steel quickly corrodes in the humid marine atmosphere. Many factors, such as relative humidity, temperature, air pollutants, and dust content, influence the atmospheric corrosion of metals [8-10].

The atmospheric corrosion of mild steel was extensively studied in the last few decades by outdoor exposure tests and traditional indoor accelerated tests like salt fog spray and cyclic wet-dry

intermittent immersion tests [11-13]. Recently, a multi-factor complex accelerated corrosion test that simulates the actual atmospheric corrosion has been developed [11,14-16]. To accurately predict the corrosion rate and corrosion behavior of mild steel in general, the corrosion tests need to provide data regarding the mass change of specimens after the removal of corrosion products. However, such measurements are not appropriate for the assessment of the early stages of atmospheric corrosion of carbon steels since the mass does not change significantly in the initial period, which might cause a relatively high measurement error.

Literature data regarding a direct measurement of the corrosion rate in the initial stages of atmospheric corrosion of mild steel obtained from simulated laboratory tests are rather scarce. In the present work, a simple experimental setup was developed, and a new analysis method based on wavelet decomposition was used to assess the corrosion rate of mild steel exposed to constant relative humidity and temperature during the early stages of the corrosion in a simulated environment. The effect of salt spray concentration on the initial atmospheric corrosion was examined.

**2. EXPERIMENTAL**

*2.1 Sample Preparation*

Table 1 shows the composition of Q235 steel. Before the experiments, a copper wire was welded to one end of the specimen, while another end of the sample was used as a working surface with a size of 50 × 3 mm<sup>2</sup>. Two identical Q235 steel electrodes with dimensions of 50 × 10 × 3 mm<sup>3</sup> were tightly packed together, and a 0.1 mm-thick polyethylene terephthalate slice was placed as insulation between the two Q235 steel specimens used as working electrodes. The distance between the working electrodes was 0.5 mm. Finally, all joints were sealed with epoxy resin (Fig. 1). Before the testing, the working surface was ground on the 800 grit silicon carbide paper, degreased with acetone, rinsed with distilled water, and dried in cold flowing air.

**Table 1.** Composition of Q235 steel (wt.%, mass fraction)

C	Si	Mn	S	P	N	O
0.16	0.20	0.61	<0.023	<0.019	<0.0045	<0.019

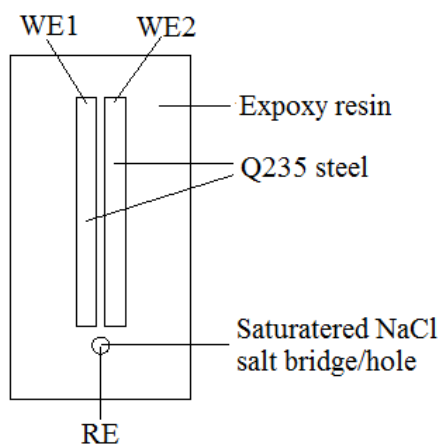


**Figure 1.** Schematic diagram of the Q235 steel electrochemical cells

The solutions of 0.01 and 0.1 mol/L NaCl, prepared using distilled water and analytical grade reagents, were used as an electrolyte.

## 2.2 Experimental setup design

The two working electrodes were Q235 samples, and the reference electrode was SCE. The important requirements for a proper self-designed electrochemical cell are stability and availability of the electrical signal even at relative humidity lower than 100 %. The distance between Q235 steel specimens was small enough. The electrochemical cell was placed in the salt spray corrosion test chamber at the exposure angle of 45°.

This salt concentration (0.01 or 0.1 mol/L NaCl) simulates the marine environment at constant temperature and relative humidity. All experiments were performed at approximately 30 °C and relative humidity of 80 % up to 168 h. The chamber, including the electrochemical cell, was placed in a Faraday cage during all EN experiments.

## 2.3 Electrochemical measurements

In the synchronized experiments, the PARSTAT 2273 Advanced Electrochemical System (Princeton Applied Research TM) in conjunction with the Power Suite software was used to conduct EN measurements using the zero resistance ammeter (ZRA) mode [17], with two Q235 steel electrodes used as working electrodes and a saturated calomel electrode (SCE) used as a reference electrode. The potential and current between the working electrodes were measured simultaneously [18]. At low frequency, the data were acquired every 0.5 s (2 Hz) for 2048 data points per data set (1024 s per data set) [19,20], while at high frequency every 0.0128 s (~78 Hz) for 10000 data points per data set (128 s per data set). The electrochemical measurements were repeated at least three times for different exposure times.

## 2.4 The surface analysis

Direct insight into the corrosion process of Q235 mild steel in the simulated environment was obtained by the exposure of Q235 steel coupons to the corrosive atmosphere at the angle of 45°. The samples were exposed for 24, 72, 100, and 148 h. The surface of the corroded coupons was examined by environmental scanning electron microscopy (XL30-TMP-ESEM). Before exposure to the corrosive environment, the coupons with a size of 50 × 10 × 3 mm<sup>3</sup> were abraded on the 800 grit sandpaper, degreased with acetone, rinsed with distilled water, dried in cold flowing air, and placed in desiccators for 24 h.

# 3. THE ANALYSIS OF THE ELECTROCHEMICAL NOISE DATA

## 3.1 Electrochemical noise resistance - $R_n$

$R_n$  represents a ratio of the standard deviation of potential noise and the standard deviation of current noise, and it was developed to determine the corrosion rate [21]. The noise resistance method is

already experimentally and theoretically approved [22-27] and used in some practical applications such as in studies of coating performance [28,29] and localized corrosion [30]. Some studies indicated that  $R_n$  and  $R_p$  are in agreement for carbon steels and stainless steels in different environments [22,31].

### 3.2 Wavelet noise resistance based on the wavelet decomposition

The window size of the wavelet analysis method [32-34] is constant, but the shape, time window, and frequency window can be varied, which represents the time-frequency localization method. The discrete sampling signal  $f(t)$  is expressed as  $\{C_n\}$ ,  $n \in \mathbb{Z}$ ; by a set of discrete filters  $H$  and  $G$ ,  $\psi_m(t)$  is expressed as  $H=\{h_1\}$ ,  $I=\mathbb{Z}$ ;  $G=\{g_1\}$ ,  $I \in \mathbb{Z}$ . The signal can be decomposed as follows:

$$ca^m_n = \sum_{k=-\infty}^{\infty} \overline{h_{k-2n}} ca^{m-1}_k \tag{1}$$

$$cd^m_n = \sum_{k=-\infty}^{\infty} \overline{g_{k-2n}} ca^{m-1}_k \tag{2}$$

The decomposition can be expressed as:

$$\begin{array}{ccccccc} ca^0 & \rightarrow & ca^1 & \rightarrow & \dots & \rightarrow & ca^{N-1} & \rightarrow & ca^N \\ \downarrow & & \downarrow & & \dots & & \downarrow & & \\ cd^1 & & cd^2 & & & & & & cd^N \end{array} \tag{3}$$

$ca^j$  and  $cd^j$  are a discrete approximation and discrete details of the  $2^j$  resolution, respectively, where  $ca^j$  is for frequencies lower than  $2^j$  part and  $cd^j$  for frequencies between  $2^j$  and  $2^{j+1}$  parts. The wavelet decomposition was applied to the current noise and potential noise which can yield different levels of discrete approximation and discrete details. The noise resistance based on the wavelet decomposition can be expressed as follows:

$$Rcd(j) = S(Ecd(j)) / S(Icd(j)) \tag{4}$$

$$Rca = S(Eca) / S(Ica) \tag{5}$$

where  $j$  is the frequency factor.  $S$  represents the standard deviation of the signal. The frequency of the decomposed signal decreases with the increase of  $j$ . When the sampling frequency is  $f$ , the signal frequency  $f_j$  of the scale  $j$  is  $f_j = f \cdot 2^j$ . The level of the wavelet decomposition of the noise resistance is an important parameter, and different decomposition levels correspond to different frequencies.

## 4. RESULTS AND DISCUSSION

### 4.1 The fluctuation of the EN

Figure 2 shows the measured values of electrochemical potential noise (EPN) and electrochemical current noise (ECN) of Q235 mild steel exposed to the simulated corrosion atmosphere of 0.01 mol/L NaCl (a1, a2, a3) and 0.1 mol/L NaCl (b1, b2, b3) for 4, 60, and 144 h, respectively. The direct current (DC) component was removed from the original EN data by using a

5<sup>th</sup>-order polynomial fitting [35]. Fig. 2 shows that the values of EPN for different times are similar to the “white noise” and also high repetition rates of potential fluctuations.

Fig. 2 (a1, a2, a3) indicates that the maximal amplitude of the EPN is 0.001, 0.001, and 0.003 V for 4, 60 and 144 h, respectively, while the maximal amplitude of ECN is 2.995, 4.258, and 12.554 nA for 4, 60, and 144 h, respectively, under the simulated corrosion atmosphere containing 0.01 mol/L NaCl. From the EPN and ECN in Fig. 2 (b1, b2, b3), we can see that the amplitudes of EPN increase from 0.0003 to 0.001 V, and the amplitudes of ECN increase from 7.823 to 19.708 nA with the immersion time. Previous studies reported that a rise in the EN amplitude originates from an increased corrosion rate [31,36]. Therefore, the obtained results indicate that the corrosion of Q235 mild steel in two simulated atmospheres progresses with time.

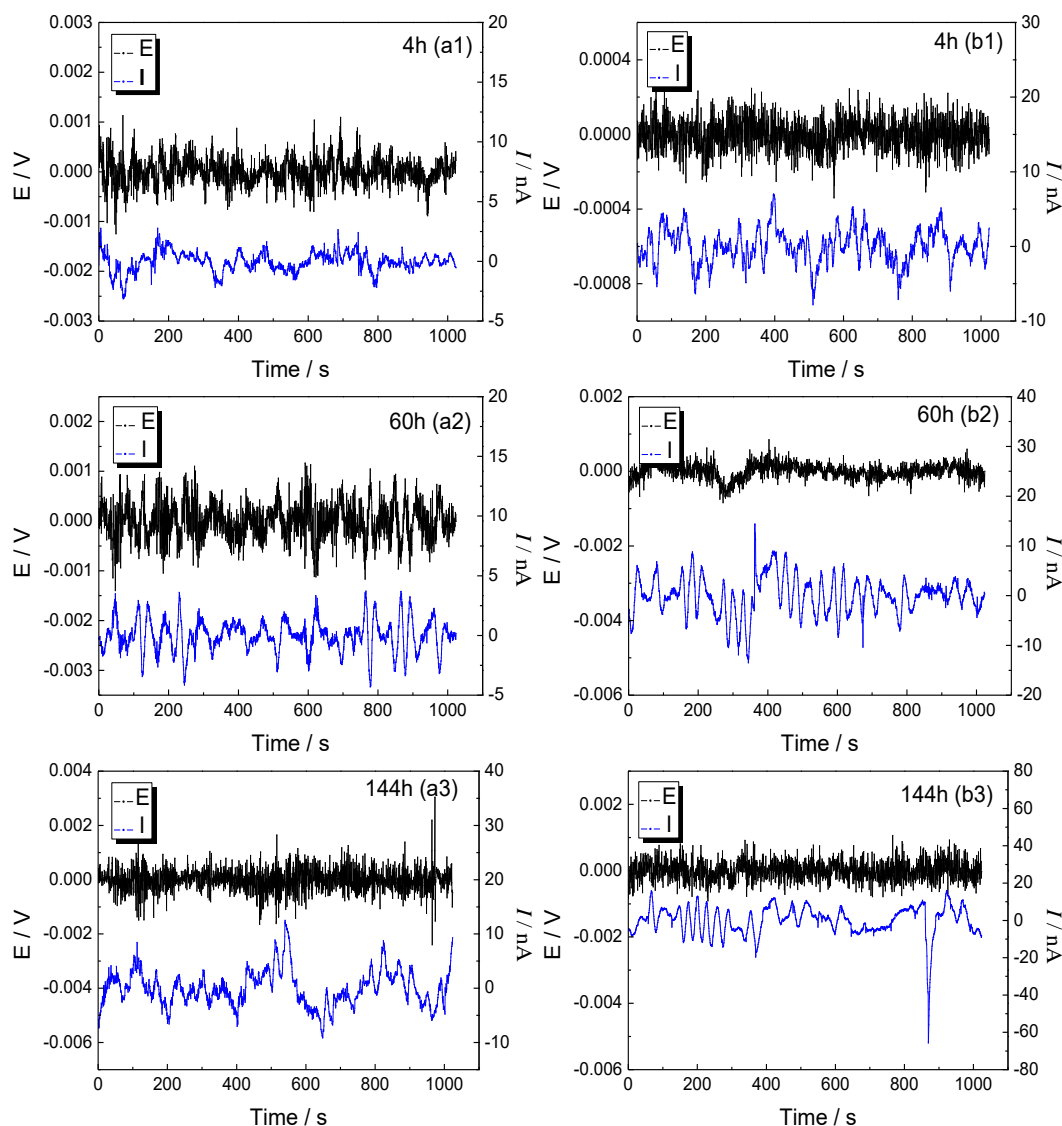


**Figure 2.** EN plots of Q235 steel in the simulated atmosphere containing 0.01 mol/L NaCl (a1, a2, a3) and containing 0.1 mol/L NaCl (b1, b2, b3) at 80% RH and 30 °C for different hours (after a dc remove by using a 5-order polynomial fitting).

4.2 The noise resistance analysis

The standard deviation of potential noise from the EN data,  $\sigma[V(t)]$ , for the investigated Q235 mild steel samples in 0.01 mol/L NaCl decreases rapidly during the initial 36 h and then slowly, while for Q235 steel in 0.1 mol/L NaCl, it slowly decreases during the entire exposure time (Fig. 3a). The standard deviation of current noise from the EN data,  $\sigma[I(t)]$ , continually increases in both simulated atmospheres (Fig. 3b). Noise resistance,  $R_n$ , defined as a ratio of the standard deviations of the simultaneously measured potential and current noise signals, significantly decreases in both simulated corrosive atmospheres in the initial 80 h, followed by a slower further decrease. As shown in Fig. 4,  $R_n$  is always lower in 0.1 mol/L NaCl than in 0.01 mol/L NaCl. Xia et al. [36,37] investigated the relation of noise resistance and corrosion of metal and found that the increase of the noise resistance reflects a decrease in the corrosion rate. Consequently, the corrosion rate of Q235 mild steel in two simulated corrosive atmospheres increases rapidly with time in the beginning and then gradually stabilizes at the later stage, Fig. 4. The results indicate that the corrosion rate with the 0.1 mol/L NaCl spraying solution is higher than that of the 0.01 mol/L NaCl spraying solution.

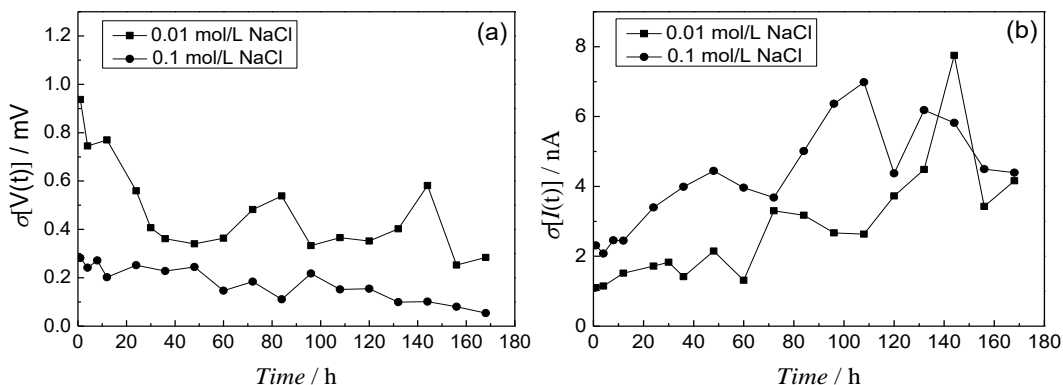


Figure 3. Standard deviations of potential (a) and current (b) for Q235 steel exposed in the two simulated atmosphere

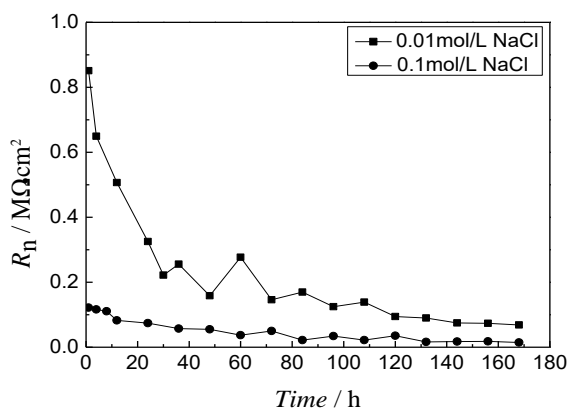


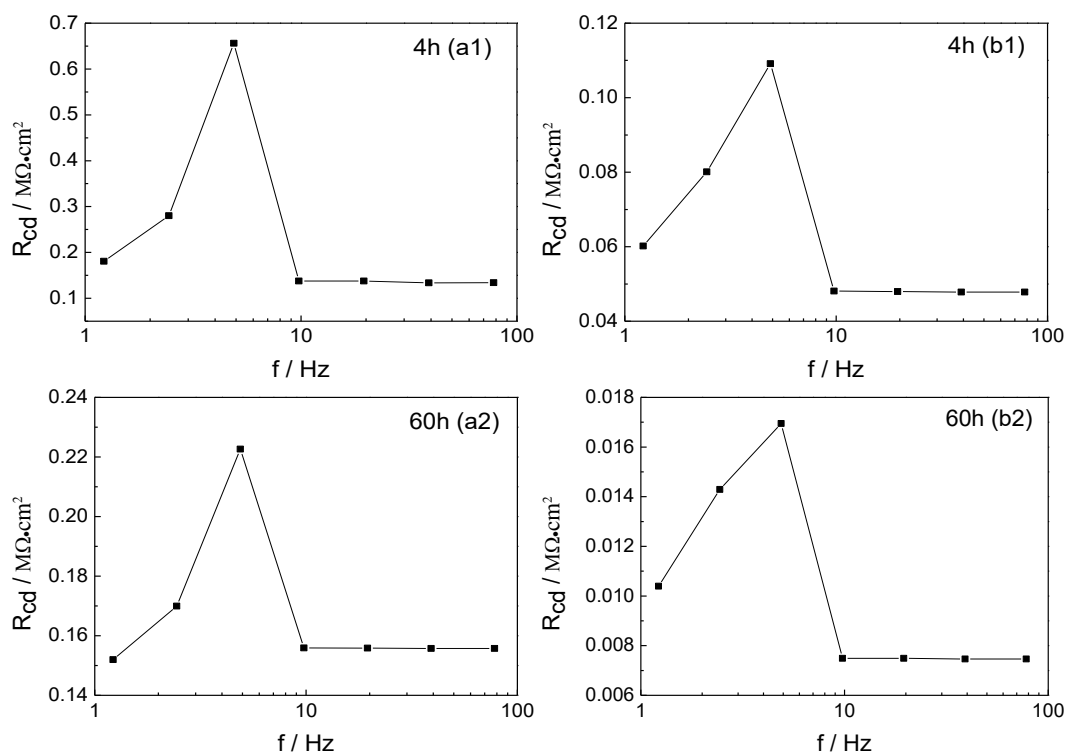
Figure 4. The noise resistance  $R_n$  for Q235 steel exposed in the two simulated atmosphere

4.3 The wavelet noise resistance analysis

The wavelet decomposition of the original high-frequency sampling signal, including the potential noise and the current noise, yield the noise resistance of different levels with sym4 wavelet

included in Matlab. The EN records were decomposed to seven levels, and the noise resistance of each level is plotted in Fig. 5. The values of wavelet noise resistance at different frequencies for Q235 mild steel after the exposure to 0.01 mol/L NaCl for 4, 60, and 144 h, are shown in Figs. 5(a1), 4(a2), and 4(a3), respectively. The values of wavelet noise resistance at different frequencies for Q235 mild steel after the exposure to 0.1 mol/L NaCl for 4, 60, and 144 h are shown in Figs. 5(b1), 4(b2), and 4(b3), respectively.

The trend of the wavelet noise resistance with the frequency was the same, increasing in the beginning and then sharply decreased, retaining a stable value with the increase of frequency. Galván-Martínez et al. [38] reported a good correlation between  $R_n$  and traditional linear polarization resistance (LPR) data. Xia et al. [31] reported that the noise resistance  $R_n$  and the polarization resistance  $R_p$  have similar physical meaning. The comparison of  $R_{cd}$  close to the frequency of 2 Hz and  $R_n$  for the two simulated atmospheres, 0.01 and 0.1 mol/L NaCl, are shown in Fig. 6(a) and 6(b), respectively.  $R_n$  and  $R_{cd}$  close to the frequency of 2 Hz have very similar values. Also,  $R_n$  and  $R_{cd}$  significantly decrease during the first 80 h, followed by a slight further decrease in both corrosion atmospheres. Therefore, the wavelet noise resistance  $R_{cd}$  can be used to accurately estimate atmosphere corrosion of Q235 steel.



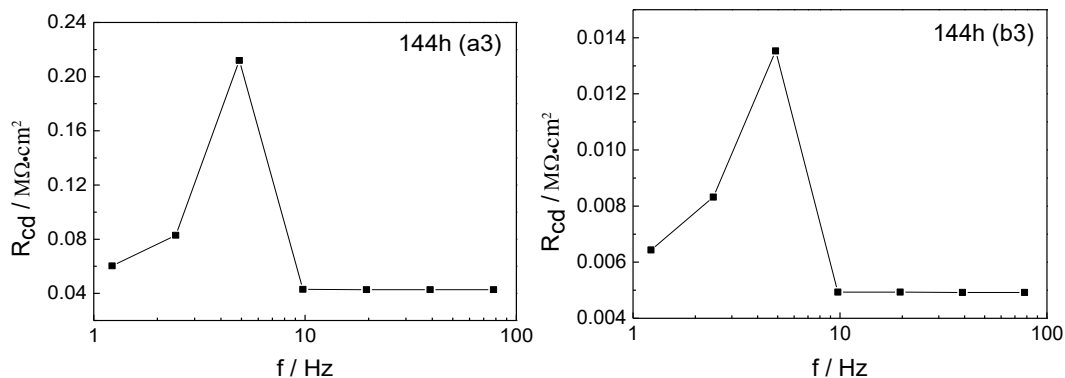


**Figure 5.** Wavelet noise resistance of the EN signals of high frequency in the simulated atmosphere containing 0.01 mol/L NaCl (a1, a2, a3) and containing 0.1 mol/L NaCl (b1, b2, b3) at 80% RH and 30 °C for different hours.

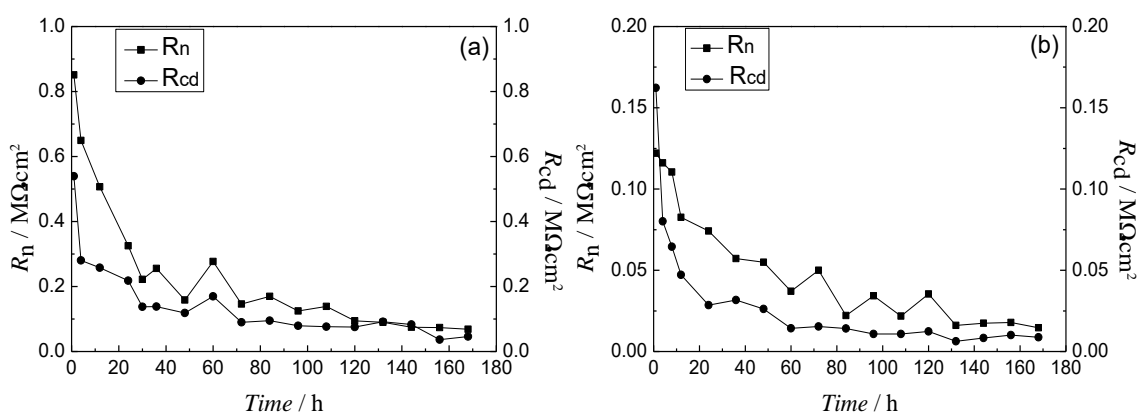


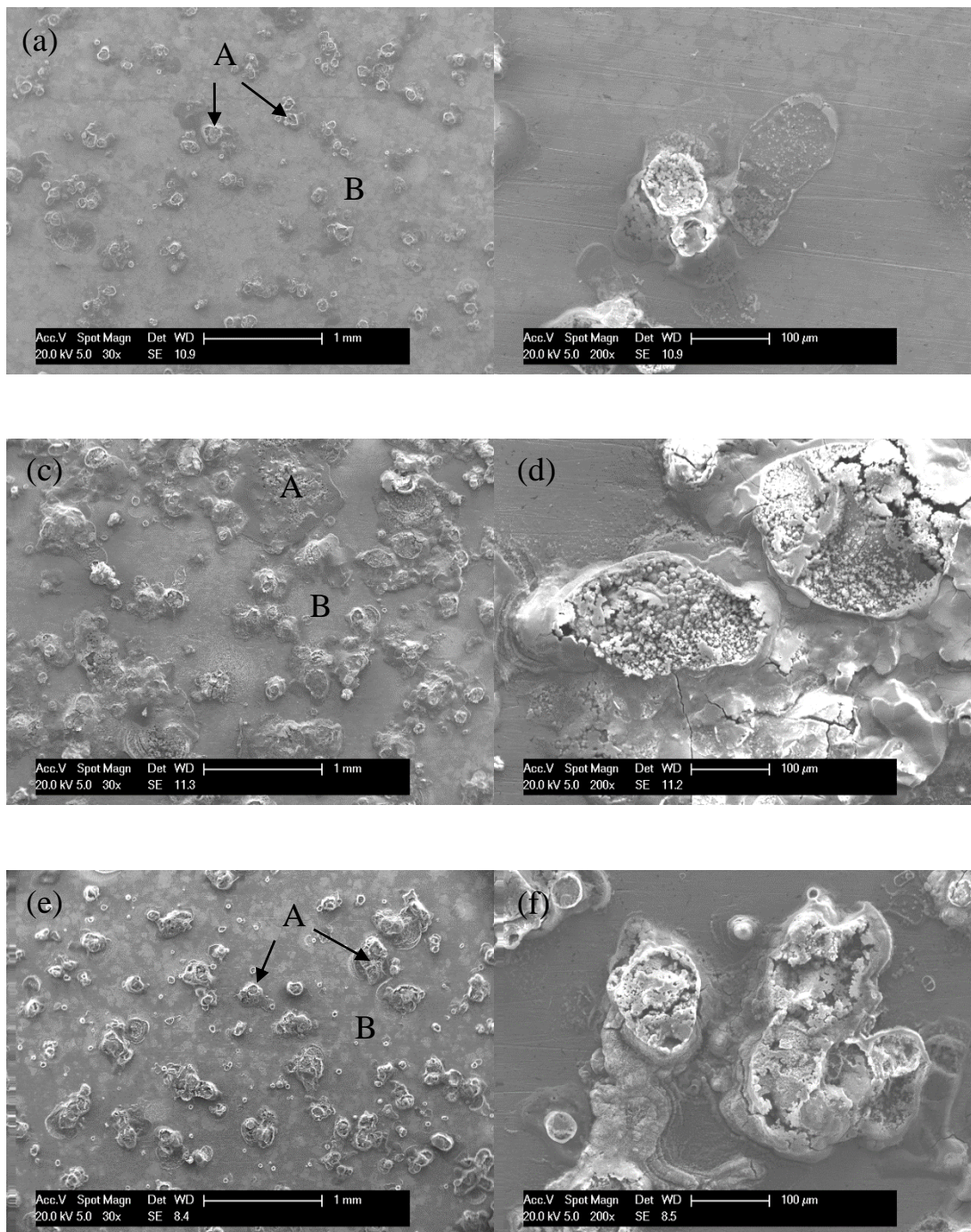
**Figure 6.** Comparison of electrochemical noise resistance and wavelet noise resistance. (a) containing 0.01 mol/L NaCl, (b) containing 0.1 mol/L NaCl.

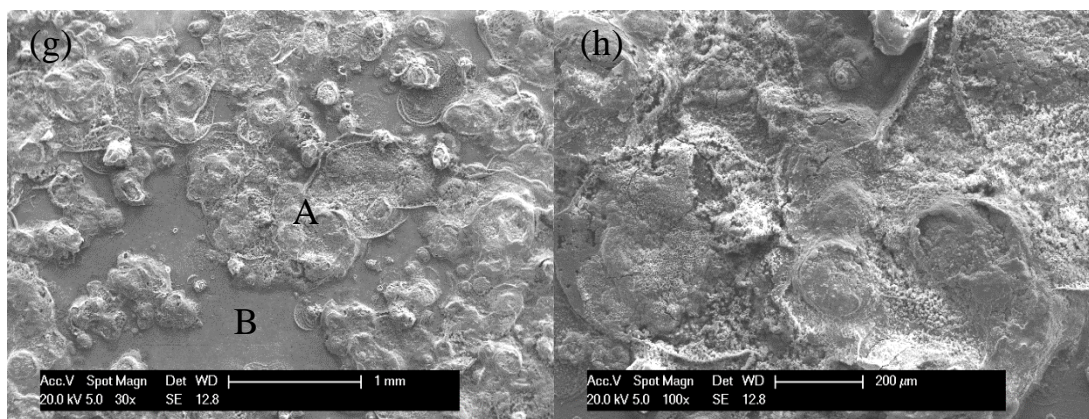
#### 4.4 Monitoring of corrosion morphology

Fig. 7 shows the SEM morphologies of Q235 mild steel exposed to the two simulated corrosion atmospheres. This experiment was conducted in an environment of the relative humidity of about 80 %. Initially, green corrosion products appeared on the Q235 mild steel surface, and then turned into brown. Eventually, the products became dark brown after a certain period. Alcántara et al. [39] reported that the dark color of corrosion products is related to the prolonged exposure time and that the chloride content in the corrosion products is high. The results of EDX analysis of the composition (atomic percent, %) at different locations on the surface are listed in Table 2. The chlorine content in corrosion products was higher than that in the area without corrosion products, confirming the previous finding.

In 0.01 mol/L NaCl, pitting morphology was observed on the surface of Q235 mild steel after 24 h, Fig. 7(a). Also, cotton-like corrosion products were found around the pitting products, Fig. 7(b). Fig. 7(c) shows significantly enlarged membrane and cellular corrosion products. The crack was found at the edge area of the corrosion products, Fig. 7(d). Furthermore, a higher amount of corrosion products, being also more prominent in size, formed on the surface of Q235 mild steel in the 0.1 mol/L

NaCl environment after the same exposure time, Fig. 7(e-h). The corrosion products gradually covered the surface by developing an interconnected network with a shell-like morphology, Fig.7, which size steadily increased until the final collapsing.





**Figure 7.** SEM images of corrosion morphology of Q235 steel. (a) Small magnification and (b) large magnification after 24 h exposed in the simulated atmosphere containing 0.01 mol/L NaCl, (c) Small magnification and (d) large magnification after 100h exposed in the simulated atmosphere containing 0.01 mol/L NaCl, (e) Small magnification and (f) large magnification after 24 h exposed in the simulated atmosphere containing 0.1 mol/L NaCl, (g) Small magnification and (h) large magnification after 100 h exposed in the simulated atmosphere containing 0.1 mol/L NaCl.

**Table 2.** EDX analysis of the corrosion products at different position in Fig.7( atomic fraction, %)

Zone	Fe	Cl	O	C	Na
A(Fig.7a)	33.95	0.47	61.28	3.30	1.01
B(Fig.7a)	88.87	-	1.26	9.87	-
A(Fig.7c)	39.50	0.17	58.62	0.72	0.99
B(Fig.7c)	88.23	0.15	7.55	3.97	0.10
A(Fig.7e)	35.28	2.04	59.21	1.51	1.96
B(Fig.7e)	97.76	-	-	2.24	-
A(Fig.7g)	38.76	1.23	58.17	0.40	1.43
B(Fig.7g)	97.85	-	-	2.15	-

#### 4. CONCLUSIONS

This paper elaborates the application of an analytical method based on the wavelet decomposition of the high-frequency noise signal to investigate the early stages of corrosion damage of Q235 mild steel exposed to the simulated corrosion environment. It was shown that the amplitude of noise signals and the noise resistance could be used to assess the corrosion rate of metallic materials. The high magnitude of noise signals and the low noise resistance indicate a severe corrosion rate. The findings of this study, namely the increase of the amplitude of noise signals and the decrease of noise resistance with the exposure time, indicate the increase of the corrosion rate of Q235 mild steel in the

simulated corrosion environment during the early stages. The value of the wavelet noise resistance closing to the 2 Hz is very close to the noise resistance. The rise in the corrosion rate with the concentration of spraying corrosion solution agrees with the results obtained by monitoring the morphology of the surface. The new analysis method of the wavelet noise resistance can be effectively used to assess the corrosion rate of Q235 steel in the early stages of atmospheric corrosion.

#### ACKNOWLEDGEMENTS

This work was supported by National Natural Science Foundation of China [grant numbers 51671144, 51871164]; Shandong Taishan Industry Leading Talents Project [grant number SF1503302301]; Science and Technology Plan Project of Tianjin City [grant number 18YFZCGX00050].

#### References

1. Z. Cui, X. Li, K. Xiao, C. Dong, Z. Liu, L. Wang, *Corrosion*, 70 (2014) 731.
2. H. Liu, F. Cao, G. Song, D. Zheng, Z. Shi, M.S. Dargusch, A. Atrens, *J. Mater. Sci. Technol.*, 35 (2019) 2003.
3. E. Schindelholz, B.E. Risteen, R.G. Kelly, *J. Electrochem. Soc.*, 161 (2014) C450.
4. M. Esmaily, P. Malmberg, M. Shahabi-Navid, J.E. Svensson, L.G. Johansson, *Appl. Surf. Sci.*, 360 (2016) 98.
5. Z. Wang, J. Liu, L. Wu, R. Han, Y. Sun, *Corros. Sci.*, 67 (2013) 1.
6. X. Lu, Y. Liu, M. Liu, Z. Wang, *J. Mater. Sci. Technol.*, 35 (2019) 1831.
7. C. Pan, W. Lv, Z. Wang, W. Su, C. Wang, S. Liu, *J. Mater. Sci. Technol.*, 33 (2017) 587.
8. M. Esmaily, D.B. Blücher, R.W. Lindström, J.-E. Svensson, L.G. Johansson, *J. Electrochem. Soc.*, 162 (2015) 260.
9. M. Esmaily, M. Shahabi-Navid, J.E. Svensson, M. Halvarsson, L. Nyborg, Y. Cao, L.G. Johansson, *Corros. Sci.*, 90 (2015) 420.
10. Y. Cai, Y. Zhao, X. Ma, K. Zhou, Y. Chen, *Corros. Sci.*, 137 (2018) 163.
11. A. Chen, F. Cao, X. Liao, W. Liu, L. Zheng, J. Zhang, C. Cao, *Corros. Sci.*, 66 (2013) 183.
12. B.O. Odio, E.C. Chinwoko, J.L. Chukwunke, J.E. Sinebe, *Int. J. Sci. Technol. Res.*, 3 (2014) 306.
13. S. Palraj, M. Selvaraj, K. Maruthan, M. Natesan, *J. Marine Sci. Appl.*, 14 (2015) 105.
14. A. Chen, F. Cao, X. Liao, W. Liu, L. Zheng, J. Zhang, C. Cao, *Corros. Sci.*, 66 (2013) 183.
15. Y. Qian, C. Ma, D. Niu, J. Xu, M. Li, *Corros. Sci.*, 74 (2013) 424.
16. L. Nie, X. Zhao, P. Liu, L. Hu, J. Zhang, J. Hu, F. Wu, F. Cao, *Int. J. Electrochem. Sci.*, 14 (2019) 3095.
17. Ł. Lentka, J. Smulko, *Measurement*, 131 (2019) 569.
18. H. Huang, X. Guo, G. Zhang, Z. Dong, *Corros. Sci.*, 53 (2011) 3446.
19. R.A. Cottis, *Corrosion*, 57 (2001) 265.
20. J. Liu, B. Chen, Y. Kou, Z. Liu, X. Chen, Y. Li, Y. Deng, X. Han, W. Hu, C. Zhong, *J. Mater. Chem. A* 4 (2016) 11060.
21. S. Girija, U.K. Mudali, H.S. Khatak, B. Raj, *Corros. Sci.*, 49 (2007) 4051.
22. C.A. Loto, *Int. J. Electrochem. Sci.*, 7 (2012) 9248.
23. M. Curioni, A.C. Balaskas, G.E. Thompson, *Corros. Sci.*, 77 (2013) 281.
24. B.P. Markhali, R. Naderi, M. Mahdavian, M. Sayebani, S.Y. Arman, *Corros. Sci.*, 75 (2013) 269.
25. S.S. Jamali, D.J. Mills, *Prog. Org. Coat.*, 95 (2016) 26.
26. J. Li, W. Kong, J. Shi, K. Wang, W. Wang, W. Zhao, Z. Zeng, *Int. J. Electrochem. Sci.*, 8 (2013) 2365.
27. S. Song, W. Zhao, J. Wang, J. Li, Z. Gao, D. Xia, *Prot. Met. Phys. Chem+*, 54 (2018) 340.

28. H. Zheng, J. Liang, Z. Qin, S. Song, L. Xu, Z. Gao, W. Hu, D. Xia, *J. Electroanal. Chem.*, 856 (2020) 113596.
29. S.S. Jamali, D.J. Mills, J.M. Sykes, *Prog. Org. Coat.*, 77 (2014) 733.
30. Y. Tan, *Sensor. Actuat. B-Chem.*, 139 (2009) 688.
31. D. Xia, C. Ma, Y. Behnamian, S. Ao, S. Song, L. Xu, *Measurement*, 148 (2019) 106946.
32. I. Daubechies, *T. Paul, Inverse Probl.*, 4 (1988) 661.
33. I. Daubechies, *IEEE T. Inform. Theory*, 34 (1988) 605.
34. Z. Dong, X. Guo, J. Zheng, L. Xu, *Electrochemi. Commun.*, 3 (2001) 561.
35. A.M. Homborg, T. Tinga, X. Zhang, E.P.M. Van Westing, P.J. Ooninx, J.H.W. De Wit, J.M.C. Mol, *Electrochim. Act.*, 70 (2012) 199.
36. D. Xia, C. Ma, S. Song, L. Ma, J. Wang, Z. Gao, C. Zhong, W. Hu, *Sens. Actuators, B* 252 (2017) 353.
37. M. Hei, D. Xia, S. Song, Z. Gao, *Prot. Met. Phys. Chem+*, 53 (2017) 1100.
38. R. Galván-Martínez, R. Orozco-Cruz, J. Mendoza-Flores, J. Genesca-Llongueras, A. Contreras-Cuevas, *Mater. Sci. Forum.*, 793 (2014) 67.
39. J. Alcántara, B. Chico, I. Díaz, D. de la Fuente, M. Morcillo, *Corros. Sci.*, 97 (2015) 74.

© 2020 The Authors. Published by ESG ([www.electrochemsci.org](http://www.electrochemsci.org)). This article is an open access article distributed under the terms and conditions of the Creative Commons Attribution license (<http://creativecommons.org/licenses/by/4.0/>).